Construction and Building Materials 389 (2023) 131739

Contents lists available at ScienceDirect

Construction and Building Materials

journal homepage: www.elsevier.com/locate/conbuildmat

Significance of macrocell currents in reinforced concrete columns partially immersed in seawater

J.R. Lliso-Ferrando [a,*], J. Soto [a], I. Gasch [a], M. Valcuende [b]

[a] Research Institute for Molecular Recognition and Technological Development (IDM), Universitat Politècnica de València, Camino de Vera, s/n., Valencia 46022, Spain
[b] Department of Architectural Constructions, School of Architecture, Universitat Politècnica de València, Camino de Vera, s/n., Valencia 46022, Spain

ARTICLE INFO

Keywords:
Macrocell corrosion
Resistivity
Reinforced concrete
Marine structures
Chlorides
Seawater

ABSTRACT

Corrosion in reinforced concrete structures located in marine environments is probably the main cause of damage, especially in elements that are partially immersed in seawater. The moisture gradient and different chloride concentrations occur in pieces under such conditions, which give way to the formation of macrocell currents between different rebar regions. Despite being studied by several authors who have run experiments in solution or with small test specimens, the significance of macrocell currents in structures has not yet been accurately quantified. The present work studied four columns that were partially immersed in seawater for more than 1 year, when the electrical resistance of concrete and the corrosion rate were monitored. After exposure, moisture and chloride content analyses were performed, and a rebar inspection was carried out. The obtained results show that macrocell currents can increase mass loss by rebar corrosion between 3- and 8-fold. They also reveal that macrocell currents can mitigate corrosion damage in areas showing cathodic performance.

1. Introduction

The degradation of reinforced concrete structures (RCS) located in marine environments has been a serious problem in civil engineering for many years due to chloride-induced rebar corrosion [1–6]. This phenomenon may lead to localised rebar cross-section loss, which may reduce the safety, aesthetics and service life of these structures [7–11].

When reinforced concrete elements are partially immersed in seawater, the portion of concrete above the water line remains non-saturated and oxygen availability is high. Nevertheless, the zone below the water line presents a high degree of saturation because it is in direct contact with seawater, and oxygen availability is lower because of low water solubility. Furthermore, this oxygen concentration lowers with depth [12]. In this region, chlorides mainly penetrate concrete by ion diffusion [9,13–18]. Directly above the water line, chlorides may also accumulate when water rises and later evaporates [19–25]. This situation can be intensified if the water level also oscillates like it does owing to tides. With all this, a moisture gradient emerges and, therefore, differences appear in the resistivity of concrete throughout elements exposed to such conditions [26]. Consequently, the rebars embedded in RCS partially immersed in seawater have different electrochemical potentials depending on each zone [21,27] (Fig. 1).

Initially, the corrosion levels of all the rebars embedded in concrete are practically negligible because a passivating oxide layer forms [28]. This layer is a very thin protective film composed of oxides and hydroxides that spontaneously emerge [29–32]. It is termodinamically stable, as Pourbaix reported in his Atlas [33]. This initial condition is not permanent. In structures located in marine environments, localised passive film breakage takes place (corrosion pits) in the rebar zones where chloride accumulation exceeds a critical level [34,35]. In these regions, kinetic activity increases because of the microcell currents generated at corroding spots [36]. Along with these microcell currents ($i_{CORR,MICRO}$), macrocell currents ($i_{CORR,MACRO}$) co-exist. The latter take place because some areas in rebars have a different electrochemical potential [27] (Fig. 2). While the whole rebar remains in the passive state, the intensity of macrocell currents is negligible due to a minor electrochemical difference among regions [36,37]. However, the intensity of these processes cannot be ignored in elements partially immersed in seawater where one rebar part is depassivated. In this case, the corroding region acts as an anode in the macrocell and the passive region displays cathodic performance. The rebar acts as a conductor of electrons, which move in the circuit, while the pore solution present in concrete acts as the electrolyte of the cell that electrochemically emerges. So to know the real rebar status ($i_{CORR,TOTAL}$), macrocells'

* Corresponding author.
E-mail address: jollife2@arq.upv.es (J.R. Lliso-Ferrando).

https://doi.org/10.1016/j.conbuildmat.2023.131739
Received 20 January 2023; Received in revised form 6 May 2023; Accepted 8 May 2023
Available online 16 May 2023

corrosive action must be added to that of microcells (Eq. (1) [36]:

$$i_{CORR,TOTAL} = i_{CORR,MICRO} + i_{CORR,MACRO} \quad (1)$$

The significance of macrocell processes in RCS has been analysed in many works. Numerous authors have opted to run tests with rebars immersed in different simulated concrete pore solutions. Andrade et al. [38] demonstrated that macrocell currents can represent between 50% and 75% of total rebar corrosion. These values are slightly higher than those obtained by Elsener [39] or Chen et al. [40], who quantified the effect of macrocell currents at between 30 and 70% and 22–67% of total rebar corrosion intensity, respectively. Chen et al. [40] pointed out that it is suitable to consider an approximate value of 38% to determine increased damage caused by corrosion because of the macrocell. Qian et al. [41] quantified this increase as being well below the previously presented values at between 1.7% and 2.4%.

More recent works [42] have observed that studies performed in solution do not actually represent how corrosion processes perform in concrete because, in this last case, the process kinetics is more limited because of the resistivity of material, and also because the coefficients of migration or diffusion of the involved species and products are lower than in solution. Duffó and Farina [43] reported that studies in solution can be useful, but extrapolation to behaviour in concrete is inadequate. In any case, the results obtained in concrete and reported by different authors are also inconsistent. For instance, Revert et al. [44] reported that macrocell currents account for between 20% and 55% of total corrosion, but these values are respectively 33% and 31% for Hansson et al. [45] and Subramaniam et al. [46]. Conversely, Rodríguez et al. [47] obtained much higher values (70%), whereas Valipour et al. [48] reported that macrocells only represent between 5 and 10% total corrosion. The marked distribution of the existing results in the literature can be justified by the different testing conditions set up by each researcher. There are major differences in the use of: sample type, resistence of concrete, cathode/anode surface ratios, exposure conditions, environmental conditions (RH and temperature), etc. This situation does not allow the significance of macrocell currents in total rebar corrosion to be clearly quantified.

Furthermore, the results obtained with small-sized samples cannot generally be extrapolated easily to real structures. For this reason, and to better understand the significance of macrocell currents in RCS, an alternative opted by some authors is to reproduce the conditions that real structures are in using scale-size pieces. This is the normal methodology in studies about the mechanical performance of structural elements [49–52]. However, research works that have focused on the corrosion process and macrocell phenomena in partially immersed elements using this methodology are scarce. Aguilar et al. [21] analysed slabs measuring 51x152x457 mm that were partially immersed in seawater, while Sagüés et al. [18] employed columns measuring 114×305×1220 mm. In both cases, the existence of macrocell currents was detected between immersed regions and those above the water line, with more serious corrosion damage for those in immersed regions than in the region near the water (evaporative or splash zone), which is usually considered to be more aggressive exposure. Walsh et al. [53,54] obtained similar results when they employed numerical models based on the field assessment of pilings from marine bridges. Despite all these works [18,21,53,54] identifying macrocell formation, none has performed a quantification of the significance of macrocell currents in total rebar corrosion.

In response to all this, the present study aimed to analyse the significance of macrocell currents in scale-size columns in such a way these currents roughly correspond to that expected for real structures located in the marine environment. To do so, four reinforced concrete columns were manufactured and partially immersed in seawater. For more than 1 year, the electrical resistance of concrete and the rebar corrosion rate were monitored at different column heights. A chloride content analysis and a moisture content study were performed at the end of the exposure period because these parameters are directly linked with corrosion processes. In addition, a visual rebar inspection was made, and mass loss by corrosion was calculated to quantify the damage caused by macrocell currents.

2. Experimental plan

2.1. Test specimens and exposure conditions

Four columns measuring 130×100×1200 mm were manufactured with steel rebars B500 SD (10 mm diameter) (Fig. 3). Rebars were arranged on the two column sides (a and b) and consisted of straight bars divided into 12 separate segments (80 mm long). The concrete cover was 20 mm and the distance between segments was 30 mm, except for the separation between levels 9 and 10, which was 150 mm. After the curing period, all the columns were partially immersed (water line as shown in Fig. 4a) in seawater, which was prepared according to ASTM D1141-98

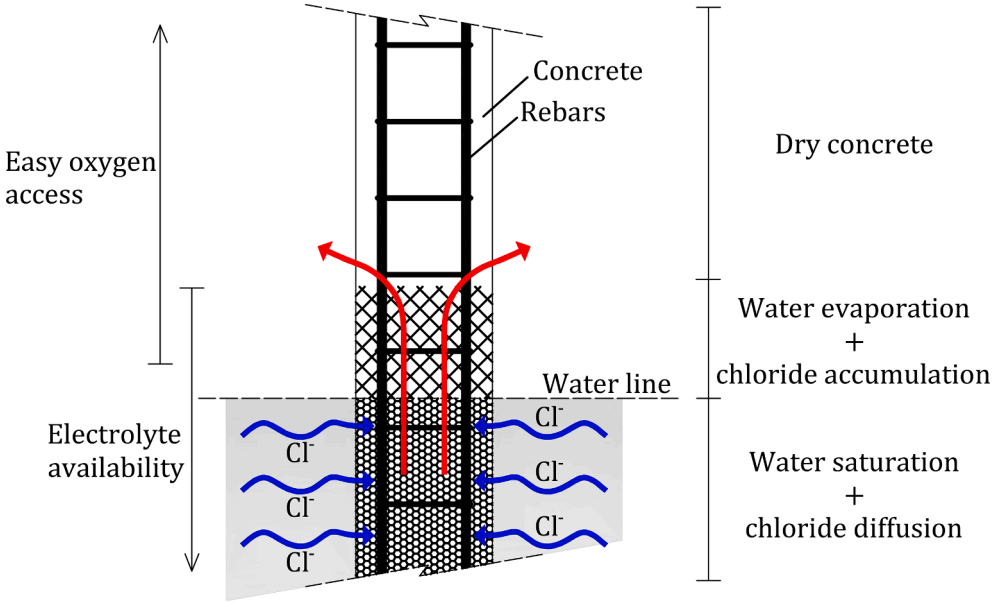

Fig. 1. Conditions in reinforced concrete columns partially immersed in seawater.

(2021) [55]. This exposure condition lasted for 407 days.

In three of the four columns (columns 1, 2 and 3), the 12 rebar segments were electrically connected to one another using wires, which were routed to a switch box to confer the rebar electrical continuity (Fig. 4a and b). The electric circuit was closed by ionic movement, which was produced through concrete thanks to the existing pore solution in the cementitious matrix. The ionic movement is conditioned by the electrical resistance of concrete. The corrosion of each segment ($i_{CORR,TOTAL}$) depends on local corrosion ($i_{CORR,MICRO}$), but also on macrocell corrosion ($i_{CORR,MACRO}$), as described in Eq. (1).

In column 4, wires remained disconnected throughout the exposure period to avoid any electric continuity among different segments (Fig. 4c). As no electrical interaction occurred among them in this case, each segment's corrosion would depend only on local corrosion ($i_{CORR,TOTAL} = i_{CORR,MICRO}$).

The nomenclature employed to designate the two column types was: "C" (electrically connected bars; columns 1, 2 and 3); "NC" (non-electrically connected bars; column 4).

2.2. Materials

The dose used to manufacture the four columns is described in Table 1. Ordinary concrete was produced, and the water/cement (w/c) ratio was 0.6. The employed cement was CEM II 32.5, with silica sand size 0/4 mm and gravel size 4/7 mm.

Test specimens were moist-cured for 28 days at 20±2 °C with RH higher than 95% before being subjected to the exposure conditions. Along with columns, samples were manufactured for material characterisation purposes. Table 2 shows the results of these tests, which were performed on the samples at the age of 28 days.

2.3. Tests

During the exposure period (407 days), the electrical resistance of concrete and the corrosion rate of the segments of each column were monitored. The following process was followed to measure both parameters:

- firstly, the current between each segment was measured by opening switches one at a time and inserting a zero-resistance ammeter (ZRA; model Keithley 2000 Tektronix) in columns 1, 2 and 3, where reinforcements remained electrically connected; C. The value was recorded 3 min after measurements commenced to ensure that the recorded signal was stable enough. The value obtained for each rebar was normalised by its surface in contact with concrete (working area, 1,571 mm^2) to obtaining the intersegment current, defined as $i_{CORR,MACRO}$.
- later, the rebar corrosion intensity ($i_{CORR,MICRO}$) of each segment was measured by the linear polarisation resistance method (LPR). This procedure is described in UNE 112072 [62]. This measurement was taken with an Autolab PGSTAT 100 Potentiostat. The Nova 1.11 software was used for signal processing. The measurement cell configuration was a 3-electrode one: each segment was the working electrode. The other column segments were utilised as the counter-electrode. The commercial MnO_2 electrodes embedded in the different column zones were employed as reference electrodes.
- the last analysed parameter was the electrical resistance of concrete at each level. All the switches between segments were momentarily opened and the conductivity (σ) between the two segments placed at the same column levels was measured by the Crison GLP-32 conductmeter model. The value was recorded 3 min after measurements commenced to ensure that the recorded signal was stable enough. Electrical resistance (R_E) was obtained by the inverse of conductivity ($R_E = 1/\sigma$).
- after taking the three measurements, the segments of columns 1, 2 and 3 were once again connected until the next measurement, while the segments of column 4 remained electrically isolated.

Once the exposure period was ended, the four columns were split open and the moisture content of concrete and the chloride content at different depths were measured. In addition, rebars were removed from columns and subjected to a cleaning process following the method described in ASTM G1-03 [63]. A visual rebar inspection was made and mass loss by corrosion was calculated.

3. Results and discussion

3.1. Visual inspection of reinforcements

Fig. 5 shows the rebars placed at the different levels of columns 2 and 4, which correspond to one C-type column and the NC-type column, respectively. It can be seen a different level of damage depending on the column type (C or NC) and the level where each rebar was located. In the C-type columns, where segments were electrically connected, there was no damage at levels 1 to 10, although pitting was detected on the rebars at levels 11 and 12. Conversely, a different pattern of damage was observed in column NC, where segments were left disconnected to avoid any electrical continuity among them. No corrosion damage was detected on the submerged rebars (levels 10 to 12), but early-stage pitting was seen on the rebar located at level 9 (aereated level, just above the water line). No damage on the other aereated levels was

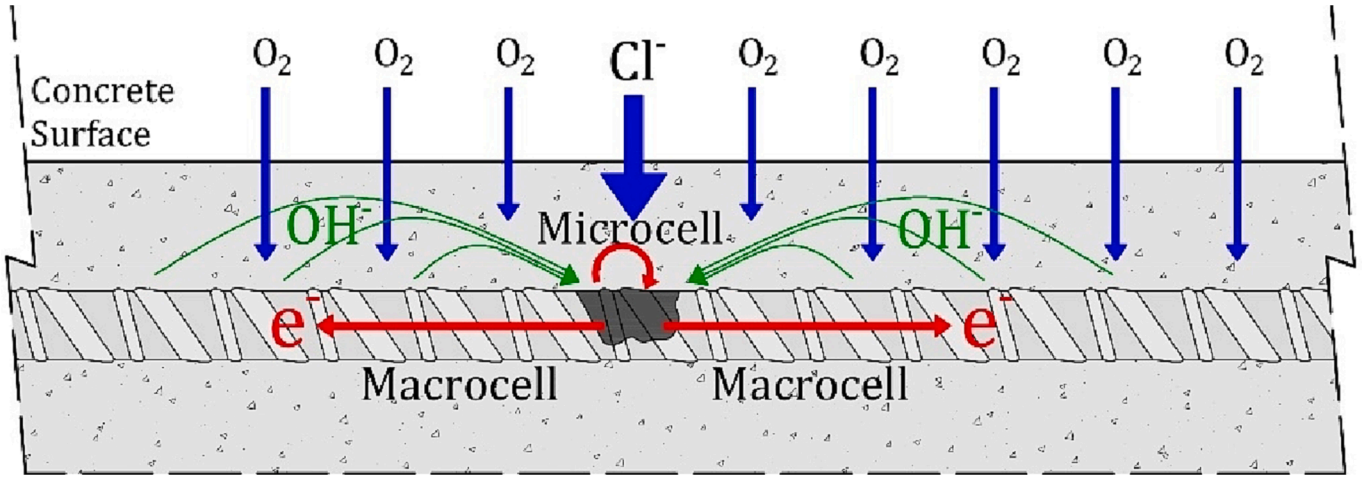

Fig. 2. Microcell and macrocell currents in reinforced concrete structures.

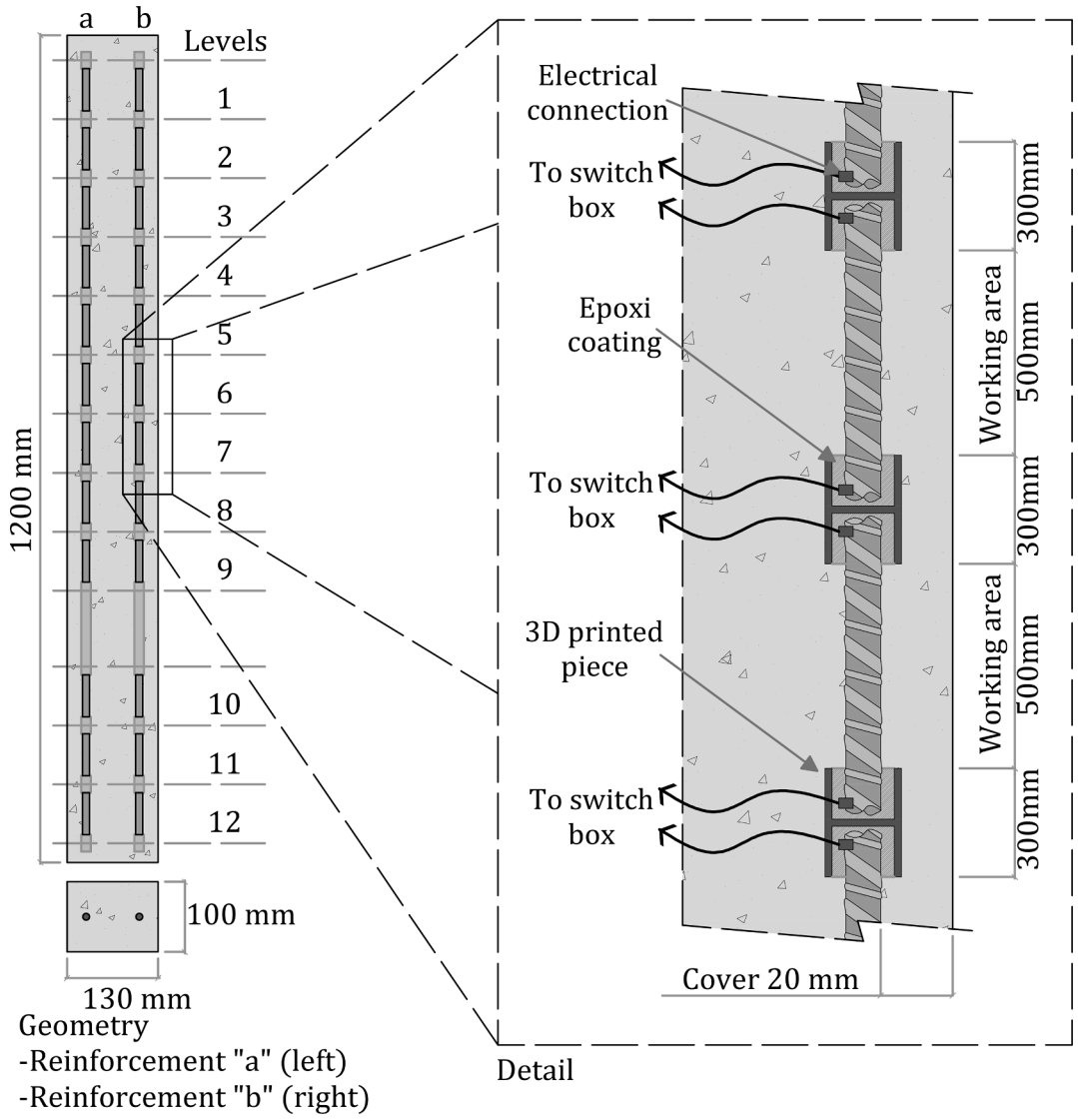

Fig. 3. Test specimen geometry and composition.

observed (levels 1 to 8) either.

3.2. Electrical resistance (R_E)

Fig. 6 shows electrical resistance (R_E) evolution at different column levels, which was similar in all the columns because it is an intrinsic concrete property.

Electrical resistance progressively increased at higher levels in all the columns as a result of continued moisture loss in these regions and gradual cement hydration from the time the curing period ended to the end of the monitoring period. The last measurements gave values that ranged between $3{\cdot}10^4$ and $6{\cdot}10^4$ Ω, which coincides with the results of other authors for measurements taken in dry concrete [64]. These data also coincide with those published by other authors who analysed electrical resistance in the aerated regions of elements partially immersed in water according to studies conducted with laboratory samples [18,21] and in real structures [65]. During the first half of the exposure period, the electrical resistance evolution at level 7 in the different columns followed the same tendency as it did at levels 1 and 4, but obtained slightly lower values (between $2{\cdot}10^4$ and $3{\cdot}10^4$ Ω). As of 200 monitoring days, this tendency changed because electrical resistance slightly lowered and was much more evident at level 9 (the aerated level, closer to the water line). In this case (level 9), this drop started as of 150 days and the values obtained at the end of the monitoring period came close to those obtained for the immersed levels (<2500 Ω). This increase in conductivity of concrete was due to higher moisture content and chlorides accumulating in this zone. The electrical resistance of concrete in the immersed zone (level 12) remained constant throughout the monitoring period with values below 1000 Ω because of the high degree of saturation [66].

3.3. Macrocell corrosion current ($i_{CORR,MACRO}$)

As depicted in Section 2.1, macrocell currents only occurred in the C-type columns (columns 1, 2 and 3) where segments were electrically connected. In column 4 (NC-type), segments were left disconnected to avoid any electrical continuity among them. Therefore, the macrocell current was null. Fig. 7 shows the macrocell current intensity evolution ($i_{CORR,MACRO}$) in the rebars of the three C-type columns. The net macrocell current was computed as the difference between the macrocell current passing through the switches below and above each segment. This measurement method has also been applied by other authors in this kind of studies [18,21].

The obtained results demonstrated that the segments of levels 11 and 12 were invariably net anodes in all cases, with macrocell currents reaching between 0.5 and 2.5 μA/cm^2 by the end of the exposure period.

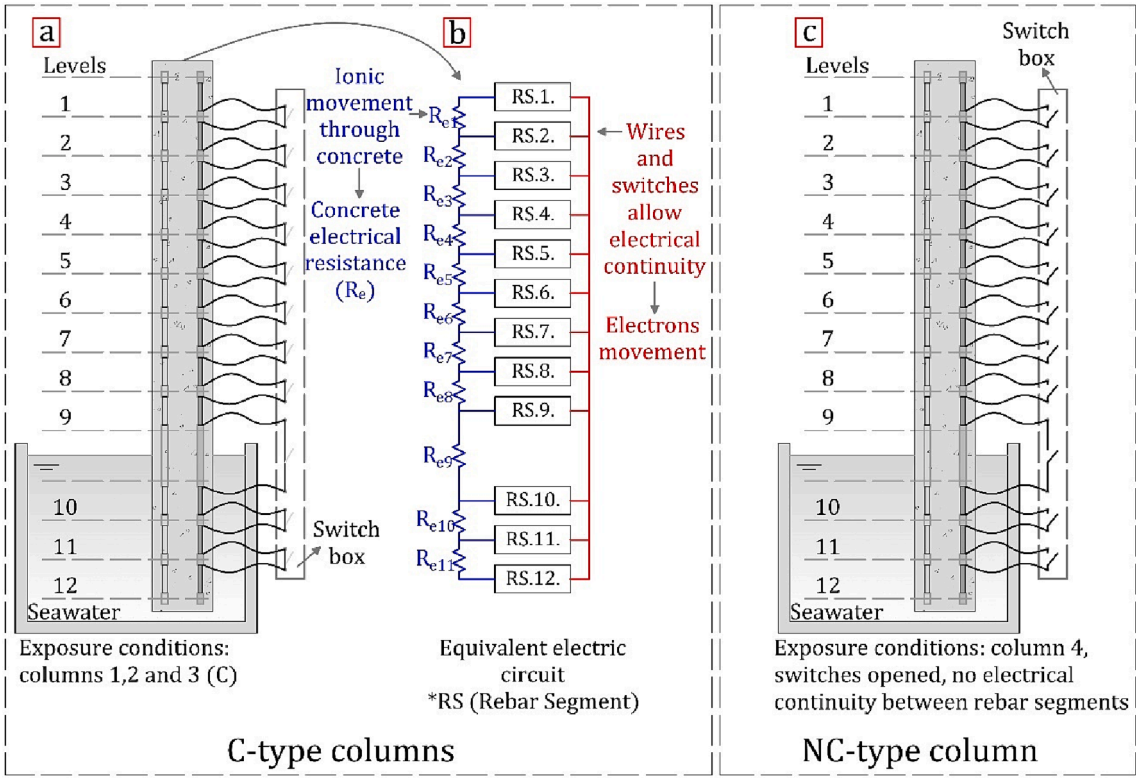

Fig. 4. Test specimen setup.

Table 1
Concrete mixture proportions (kg/m^3).

Cement	Water	Sp*	Sand (0/4)	Gravel (4/7)	w/c ratio
307	*184*	*1.85*	*1438*	*491*	*0.6*

*Sika®ViscoCrete®-20 HE superplastificiser.

Table 2
Concrete characterisation results.

Test (Standard)	Results
Compressive strength (UNE-EN 12,390 [56])	30.6 MPa
Porosity accessible to water (UNE-EN 83,980 [57])	15.8%
Capillary suction (UNE-EN 83,982 [58])	72.7 kg/m^{2}min$^{0.5}$
Air permeability (UNE-EN 83,981 [59])	$2.4{\cdot}10^{-16}$ m^2
Chloride migration, D_{nssm} (NT-Build 492 [60])	$5.4{\cdot}10^{-11}$ m^2/s
Chlroride diffusion, D_{nss} (UNE-EN 12390–11 [61])	$6.9{\cdot}10^{-11}$ m^2/s

It was at these levels where corrosion damage was detected during the visual inspection (Fig. 5). Conversely, in most cases level 10 performed as a cathode. Despite being an immersed segment, and given its closeness to the aerated zone, the oxygen concentration in water was higher than in deeper zones [12]. This generated oxygen concentration differences, which led an electric current to flow in rebars from the zones where this concentration was lower to those where it was higher. Previous studies by authors like Gartner et al. [67], who analysed 3-metre long columns (150x150x3000 mm) partially immersed in seawater, have also detected this phenomenon, although they do not quantify the significance of macrocell currents in relation to total corrosion.

The segments of levels 8 and 9 were invariably net cathodes. The oxygen and electrolyte availabilities due to diffusion and capillary suction, and their closeness to anodic regions, gave way to a reduction in the oxygen in this rebar region with electrons from immersed zones. In these segments, the $i_{CORR,MACRO}$ values were between −0.5 and −1.5 μA/cm^2 by the end of the monitoring period (negative because of the cathodic character and the established signs criterion). For higher levels (1–7), a gradual drop in cathodic activity occurred with increasing elevation. In this case, the greater electrical resistance at these levels and the progressive increase in the distance to anodic regions (immersed zone) favoured the scarce participation of the segments located at these levels in macrocell processes. As of level 5, the $i_{CORR,MACRO}$ values remained constantly below −0.1 μA/cm^2 throughout the monitoring period. By way of example, Fig. 8 shows $i_{CORR,MACRO}$ evolution at each rebar level of Column 1b.

The results shown in Fig. 8 reflect the difficulty of clearly defining the existence of anodic or cathodic regions on the first 30–40 days. At the end of the curing process, all the segments were in the passive condition. In this situation, the repercussion of macrocells was negligible, as reported in previous works [37,42]. However, these studies were carried out in simulated concrete pore solutions [42] or using small test specimens [37], where macrocell currents may be different from those in real structures. This was due to the similarity of the electrochemical potential of the different segments, while their initial passivity condition remained in them all. However, this tendency drastically varied as of 50 days. At level 12, abrupt net electron generation onset (anodic performance) took place, which also occurred later at level 11, but less intensely. At the same time, both levels 9 and 10, and level 8 to a lesser extent, were clearly identified as net electron consumption regions (cathodes). This performance can be explained by analysing the sequence in which processes took place during the exposure period. When partially immersing columns, upper parts began to dry and lower parts increased the moisture content by creating a moisture concentration gradient. These conditions allowed chloride diffusion in the zones below the water line and, albeit much more slowly, chloride accumulation also occurred immediately over the water line due to a rise in seawater because of diffusion and capillarity. Depassivation due to a higher chloride content took place in the segments located at lower levels (as of 50 days in this case), which produced metal oxidation and a source of electrons to emerge for the rebars that remained under the

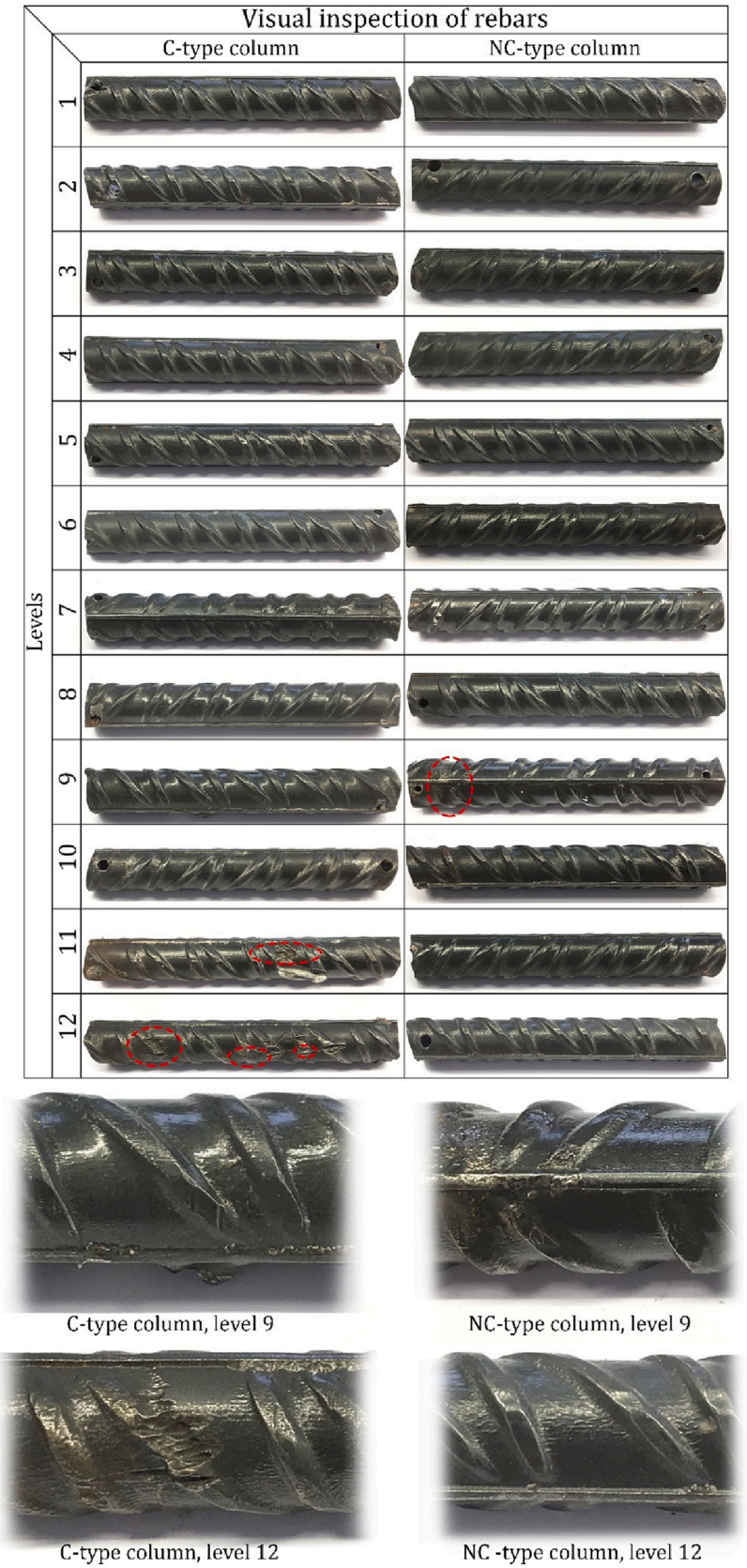

Fig. 5. Visual inspection of rebars depending on column height (level) and type (C or NC).

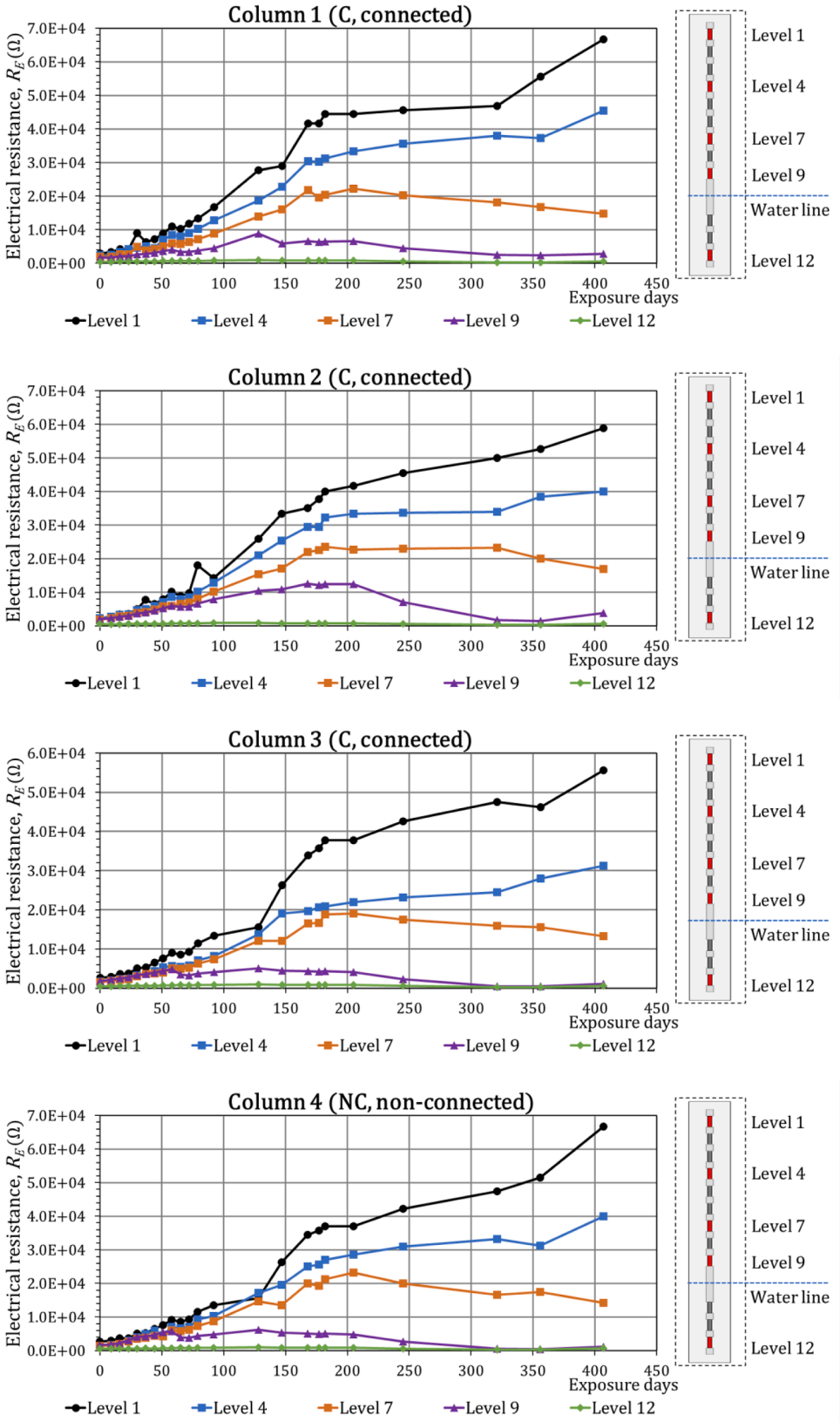

Fig. 6. Electrical resistance of concrete at different levels during the exposure period.

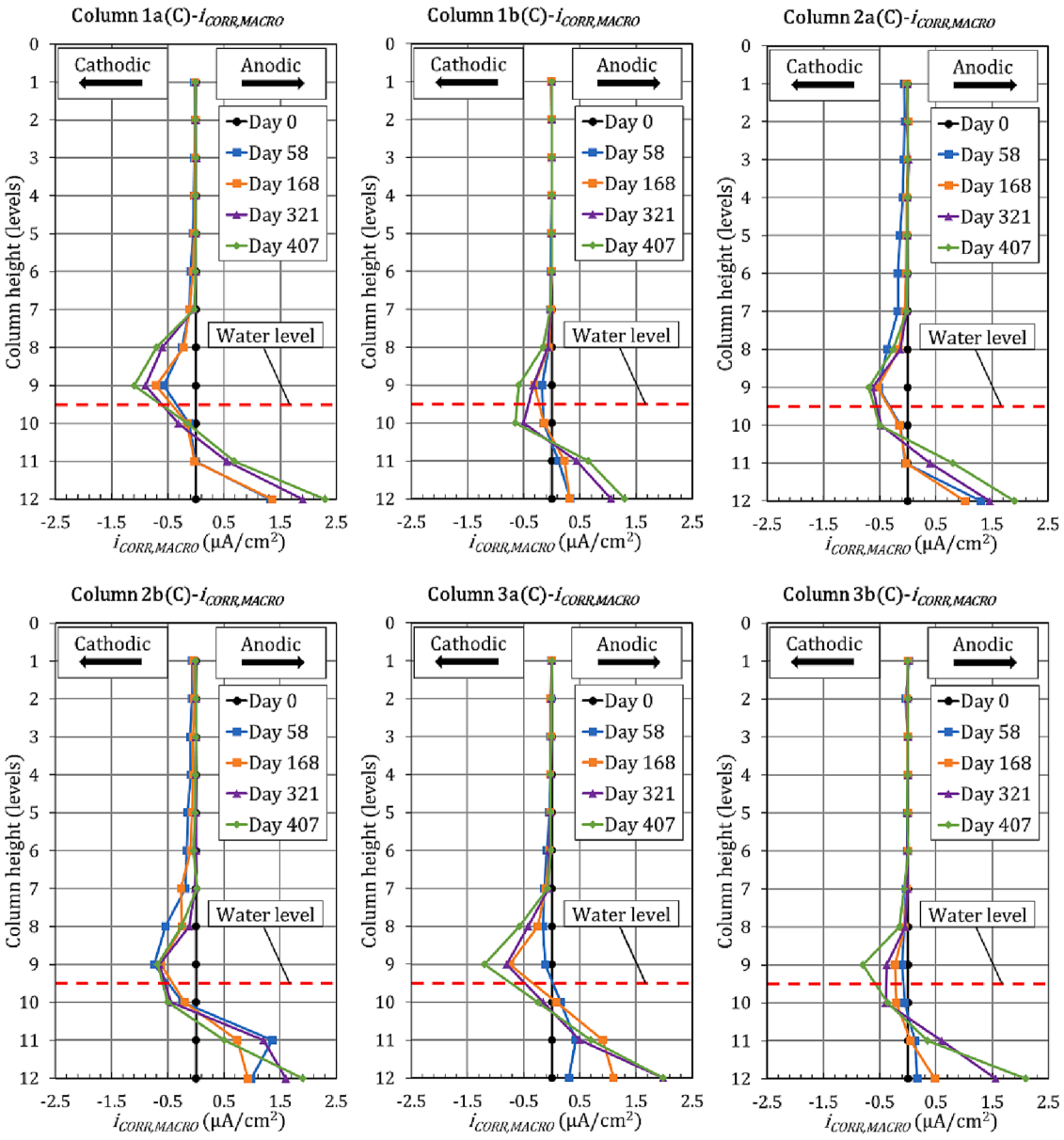

Fig. 7. Macrocell corrosion ($i_{CORR,MACRO}$) evolution in different columns.

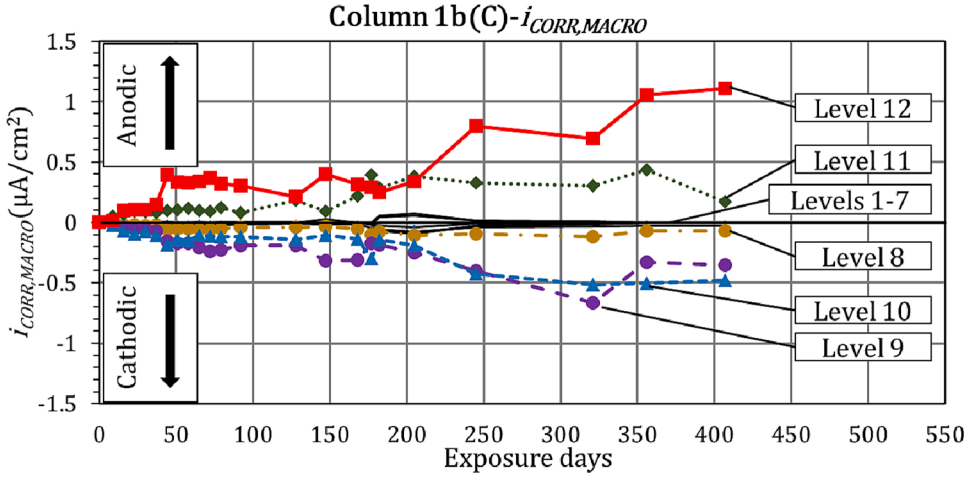

Fig. 8. Macrocell corrosion ($i_{CORR,MACRO}$) evolution in Column 1b during the exposure period.

passive condition. As the closest zone and that with greater oxygen availability corresponded to those of the segments located at levels 8 to 10, the cathodic reaction took place immediately above the water line, as shown by the macrocell current corrosion in Fig. 8. This was observed by other authors in tests performed on small slabs [21], although neither the corrosion rate nor significance of macrocell currents were determined in this study.

Fig. 8 also shows the scarce participation in the macrocell processes involving the rebars located at levels 1 to 7, which is observed in the graphs of Fig. 7 as well.

3.4. Microcell corrosion current ($i_{CORR,MICRO}$)

Fig. 9 depicts the corrosion intensity evolution of each analysed segment ($i_{CORR,MICRO}$) in the four columns. At the beginning of the exposure period (age 0), the recorded $i_{CORR,MICRO}$ value was lower than 0.1 μA/cm^2 in all cases. This fact denotes the initial passivity of metal and lack of corrosion at the end of the curing process [68]. Later measurements revealed a generalised drop in the local corrosion intensity in the segments from levels 1 to 7 of all the columns regardless of C or NC types. Reduced moisture in all these regions and lack of chlorides favoured this scenario. Moreover, at levels 8–10, the $i_{CORR,MICRO}$ values increased because chlorides were present and, in this case, differences among columns were clearly seen. At the end of the exposure period, in the C-type columns (columns 1, 2, 3) the segments at levels 8 and 9 still had a negligible corrosion level with $i_{CORR,MICRO}$ values below 0.1 μA/cm^2. Nonetheless, values were over 0.6 μA/cm^2 in the NC-type column (column 4), which means that the passivating oxide layer that protected rebars had been destroyed and corrosion onset had begun [68]. These differences appeared between the C- and NC-type columns because no depassivation had taken place in the former type (columns 1, 2, 3) thanks to more steel protection at levels 8 and 9 as a consequence of them participating as cathodes in macrocell processes, which the previous section indicates (Fig. 7 and Fig. 8). In other words, the contribution of the electric charge from anodic regions (lower levels) enhanced steel protection by reducing, or even inhibiting, the oxidation process. This fact was also noticeable with the rebars located at level 10.

For the segments located at levels 11 and 12, a notable difference was found between the C-type columns (columns 1, 2, 3) and the NC-type column (column 4). In the NC-type column, the values for the segments placed at these levels went from 0.1 to 0.5 μA/cm^2 at the end of the monitoring period, which represent a moderate corrosion level according to Standards UNE 112072:2011 [62], RILEM TC-154-EMC [68] and ASTM STP 1065 [69] (Fig. 10b). Nonetheless, much higher values were obtained in the C-type columns, which went from 0.5 to 8 μA/cm^2, and denote a high corrosion level (Fig. 10a). This greater corrosion was due to the influence of macrocell currents, which occurred only in the C-type columns. According to what Section 3.3 states, the segments at levels 11 and 12 acted as anodes and, therefore, conferred an electrical charge at higher levels that led to a faster corrosion rate. All these data coincided with the damages observed during the visual inspection of the reinforcement at the end of the exposure period. In the C-type columns, pitting was detected on the rebars at levels 11 and 12, but no damage was noted at the same levels on NC-type column. Early-stage pitting was detected at level 9 on the NC-type column, but no damage was noticeable on the C-type column at the same level.

In the graphs in Fig. 10, differences between column types (C or NC) also appeared for corrosion onset age. In the segments at levels 11 and 12 of the C-type columns (Fig. 10a), corrosion onset began before 35 days and the $i_{CORR,MICRO}$ values were higher than 0.2 μA/cm^2 (the threshold at which steel depassivation occurs [68]). Conversely with the NC-type column (Fig. 10b), corrosion onset occurred later, as of 75 days. These data reveal that macrocell processes influenced not only rebars' kinetic activity, but also the corrosion onset period. This was because chloride ions (negative electric charge) were attracted by metal, which had a positive electric charge as a result of the macrocell current. Thus, when a macrocell current was present, the chloride diffusion process was also empowered by the migration process. This hypothesis has been previously observed [37], nevertheless this study was performed in small test specimens, where macrocell currents are often lower than in real structures.

3.5. Moisture content

At the end of the exposure period, moisture content was obtained by following the gravimetric method (weight change following 168 h at 45 °C) of the bulk samples obtained from different column heights. This method is described in [70,71] and some authors have used it for similar experiments [21]. By way of example, Fig. 11 shows the results obtained in column 1. These results reflect a high degree of saturation in the immersed zone, while moisture content at higher levels gradually dropped with height. At levels 1–6, moisture content was almost 10-fold lower than in the immersed zone. As a consequence of these differences in moisture and, therefore, in oxygen availability, plus the differences in chloride content (see Section 3.6), rebar segments reached distinct electrochemical potentials, which gave way to macrocell currents appearing as long as segments were interconnected.

3.6. Chloride content

The chloride content analysis was carried out at different depths with the drilled-out samples taken at distinct column levels at the end of the exposure period. The chloride content measurement was taken in accordance with the procedure described in Standard NTBuild 208 [72]. Fig. 12 contains the obtained results. This figure also shows the critical chloride content threshold (C_{crit}) at which rebar depassivation takes place according to the bibliography. Although discrepancies appear for different authors [34,73–76], they tend to take C_{crit} values between 0.6% and 1.0% per cement weight.

At levels 1–7, chloride content in all the columns was residual. These chlorides came from the materials used to manufacture concrete. In the closest aerated zone to the water level (level 9) and at the immersed levels (levels 10, 11 and 12), chloride content was much higher than the critical threshold. Level 9 was also where the chloride concentration of the whole column tended to be the highest, probably because it was the evaporation zone of the water from immersed zones and, therefore, where chlorides were deposited while water outwardly migrated. Other authors like Gartnet et al. [67] have also observed this in structures partially immersed in seawater. Liu et al. [77] have obtained similar results with numerical analysis models.

Fig. 12 shows that the values obtained at levels 11 and 12 for the C-type columns were higher (average of 30%) than those for the NC-type column. These differences can be justified by the fact that the macrocell currents that existed in the C-type columns generated greater anodic polarisation in active rebar zones, which favoured chloride migration (negative electrical charge) towards the steel surface [37].

Although there is a very high chlorides concentration at levels 9–12, the macrocell currents have conditioned the location of the areas where corrosion has occurred. Thus, for example, in contrast to the NC-type column, no damage was found on the rebars of the C-type columns at level 9 because rebars' protection increased thanks to the supply of electrons from the bars located in immersed zones, as this region (level 9) acted as a cathode in macrocell currents (Fig. 5 and Fig. 7). Hence the electrons loss that resulted from local corrosion diminished in accordance with Eq.1 and resulted in less local corrosion.

3.7. Mass loss due to corrosion

The objective of this study was to quantify the real influence that macrocell currents have on total rebar corrosion in structures found in marine environments. To do so, using the data presented in Sections 3.3

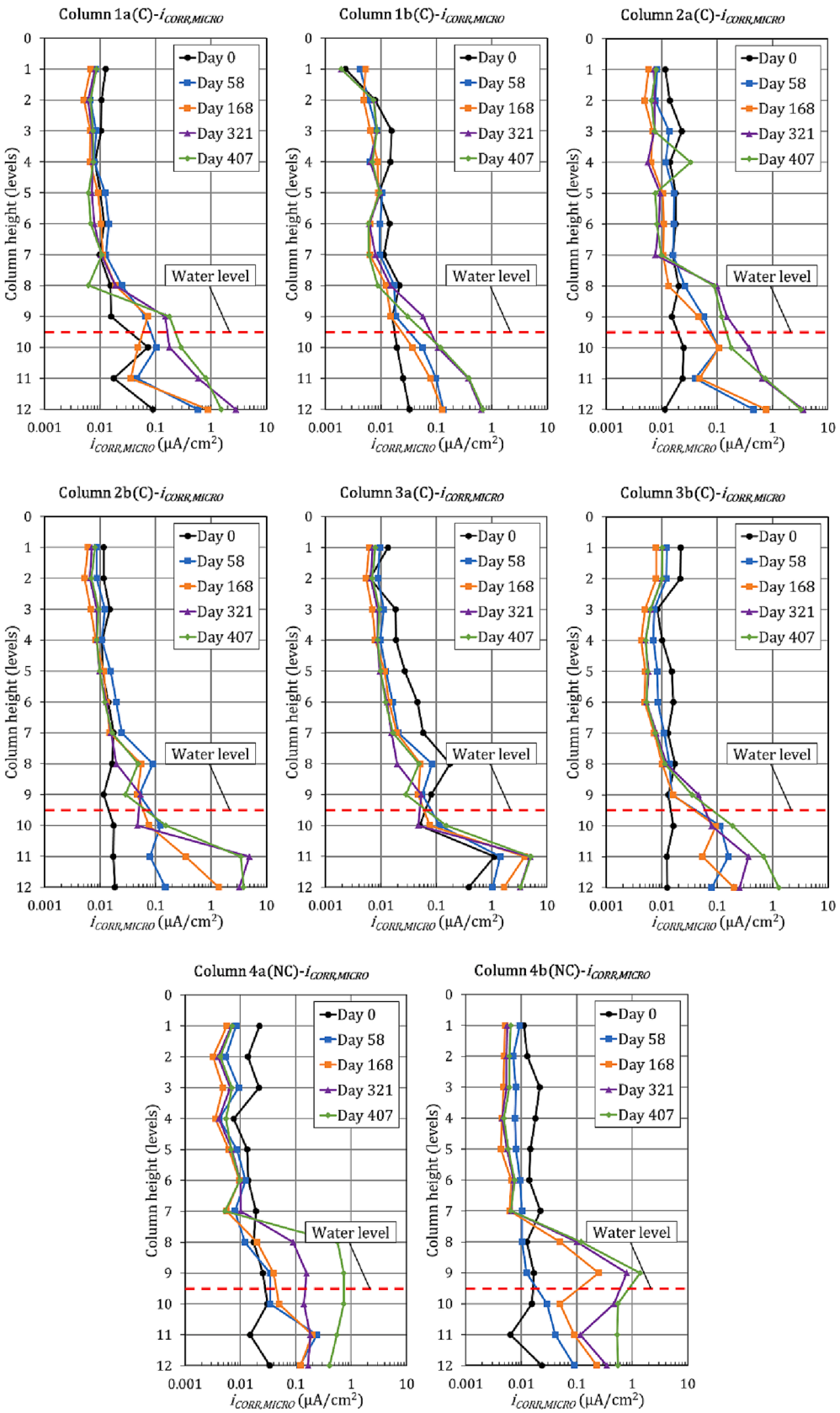

Fig. 9. Microcell corrosion ($i_{CORR,MICRO}$) evolution during the exposure process.

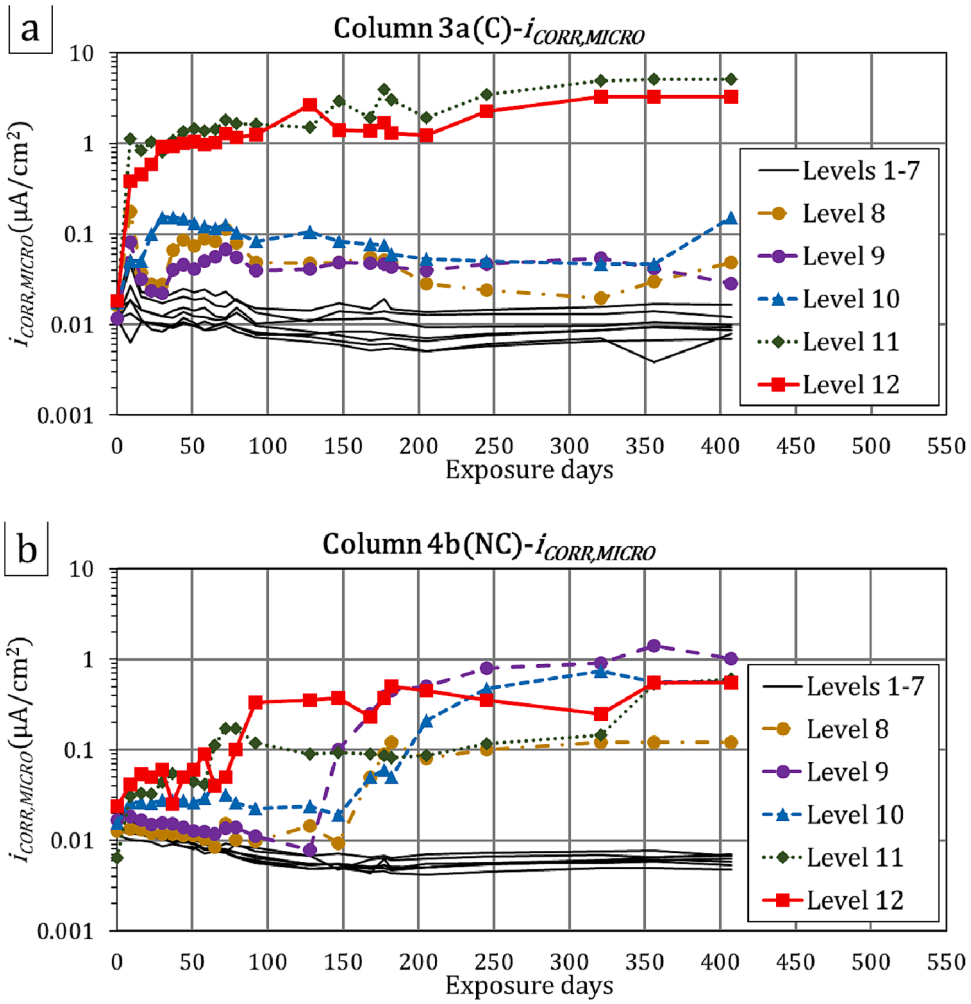

Fig. 10. Microcell corrosion ($i_{CORR,MICRO}$) evolution in: (a) C-type column (3a) and (b) NC-type (4b).

and 3.4, the total corrosion intensity ($i_{CORR,TOTAL}$) of each segment making up the rebar of every column was calculated as set out in Eq.1. In the C columns, where the different rebar segments were electrically interconnected, the corrosion of each segment was the sum of local corrosion ($i_{CORR,MICRO}$) and macrocell corrosion ($i_{CORR,MACRO}$) (Fig. 13a). In the NC column with no macrocell currents, total corrosion was that corresponding to local corrosion ($i_{CORR,MICRO}$) (Fig. 13b).

Once the total corrosion intensity evolution of each rebar segment was known by integrating the $i_{CORR,TOTAL}$-time curve, the mass loss ($\Delta m, calc$) that accumulated during the exposure period was estimated in accordance with Faraday's law (Eq. (2), as shown by:

$$\Delta m, calc = \frac{M}{n \cdot F} \cdot \int_{t_0}^{t} i_{CORR} \cdot dt \tag{2}$$

where M is the steel atomic mass (55.845 g/mol), t is the time in seconds, n is the number of electrons released or acquired during the corrosion process (2 for this case) and F is Faraday's constant (96845 C/mol). Mass loss ($\Delta m, calc$) was obtained as g/cm^2 and was, thus, normalised by the rebar surface (1,571 mm^2).

Fig. 14 shows the average mass loss per segment value. The results are logarithmically presented to facilitate their reading.

Fig. 14 clearly shows the significance of macrocell corrosion currents, especially in immersed regions; that is, those participating in macrocell proceses as anodes. For example, at level 12, the average steel loss of the rebar segments submitted to macrocell currents (column C) was 236 mg (more than 400 mg in some cases) but was 30 mg for the segments at the same level that did not participate in macrocell processes (the NC column), which was practically 8-fold lower. A similar situation was noted at level 11 with mass loss in the segments that participated in the macrocell processes being 3-fold higher than for the same segments that did not participate in such processes (129 vs. 43 mg). These records coincide with the damage observed during the visual inspection of the reinforcement at these levels. Significant pits were detected in the C-type column, while no damage was found at the same levels in the NC-type column (Fig. 5). In addition, these data showed the strong influence that macrocell currents had on $i_{CORR,TOTAL}$ in anodic regions, which could multiply steel loss by between 3- and 8-fold and, therefore, corrosion damage. These data were much higher than those collected from works in the literature about small-sized samples, which quantified the maximum of macrocell significance in corrosion damage as 65–70% of total corrosion [39,40]. Unlike these works, elements made to scale were employed, which were able to reproduce the conditions that occur in RCS exposed to marine environments more closely to reality.

In the segments at level 10, where macrocell currents were very low (Fig. 7), no clear differences could be established among columns because mass loss was similar in columns C and NC with 35 mg and 38 mg, respectively.

At levels 8 and 9, and unlike what happened at levels 11 and 12, the mass loss in the bars submitted to macrocell currents (C-type columns) was virtually null (<1 mg) and was much lower than that obtained for the NC column rebars without macrocell currents. In the latter column

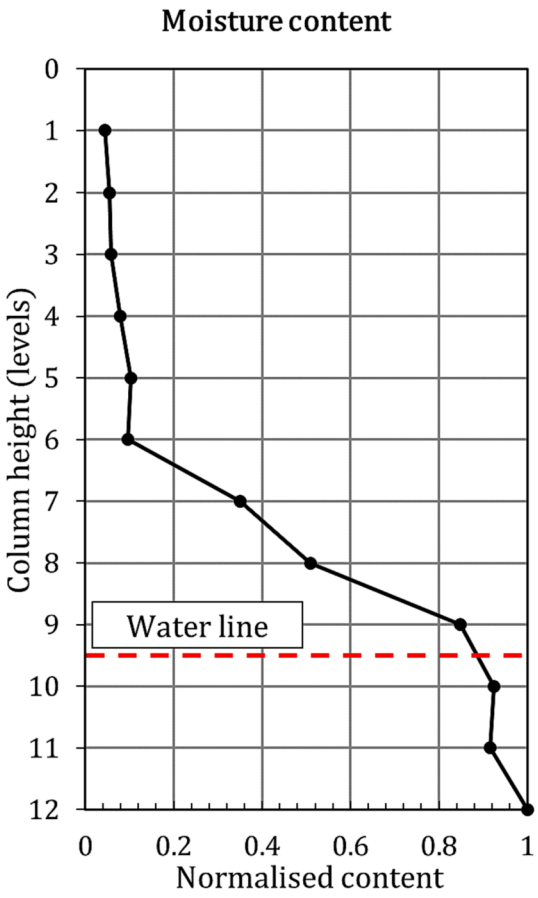

Fig. 11. Normalised moisture content from Column 1.

type, the average mass loss was respectively 12 mg and 85 mg at levels 8 and 9; that is to say, more than one order of magnitude for the difference with the rebars of the C columns. As Section 3.3 informs, the rebars of the C columns located at these levels acted as cathodes in macrocell corrosion processes, which counteracted the electrons loss that took place by local corrosion and led to less total corrosion. In short, these data demonstrated that macrocell currents increased corrosion in some structure zones, but reduced it in others. This is again in line with that observed during the visual inspection (Fig. 5). No damage was detected at these levels (8 and 9) on the C-type column, but early-stage pitting was detected at level 9 on the NC-type column.

In the rebars located at levels 1–7, mass loss was practically null in all cases (almost the same or below 1 mg). Lack of chlorides and greater concrete resistivity in these regions favoured no active corrosion processes taking place in these stretches, which resulted in substantial mass loss. No damage was detected during the visual inspection in the rebars at these levels on both the C-type and NC-type columns.

4. Conclusions

In RCS partially immersed in seawater, both a moisture gradient and chloride concentration occur, which give way to macrocell currents. Four scale-size columns were used in this study in such a way that the macrocell currents roughly corresponds to that expected for real structures located in the marine environment. The columns were partially immersed in seawater for 407 days. The obtained results allow the following conclusions to be reached.

1. The macrocell currents have a strong influence on the corrosion. The corrosion rate in anodic areas increased by more than one order of magnitude related to identical rebars that did not take part in macrocell processes (0.5 to 8 μA/cm^2 vs. 0.1 to 0.5 μA/cm^2). As a consequence, steel mass loss by corrosion was almost 8-fold higher in some immersed zones at the end of the testing period.
2. In the closest aerated zone to the water line, where the chloride content and the microcell corrosion are very high, the macrocell current also has a strong influence. This current acts by bringing electrons from the more submerged area (which counteract the electrons loss by microcell corrosion), with values between −0.5 and −1.5 μA/cm^2 by the end of the monitoring period. As a result, the total corrosion rate was negligible (below 0.1 μA/cm^2) and the steel mass loss by corrosion was reduced by about two orders of magnitude related to identical rebars that did not take part in macrocell processes.
3. The participation of the rebars located in the aerial zone that act as cathodes diminishes as the distance to the water surface grows owing to resistivity of concrete. From 30 to 40 cm above the water level, the recorded macrocell currents were lower than 0.1 μA/cm^2 (almost negligible) by the end of the study period in all cases.

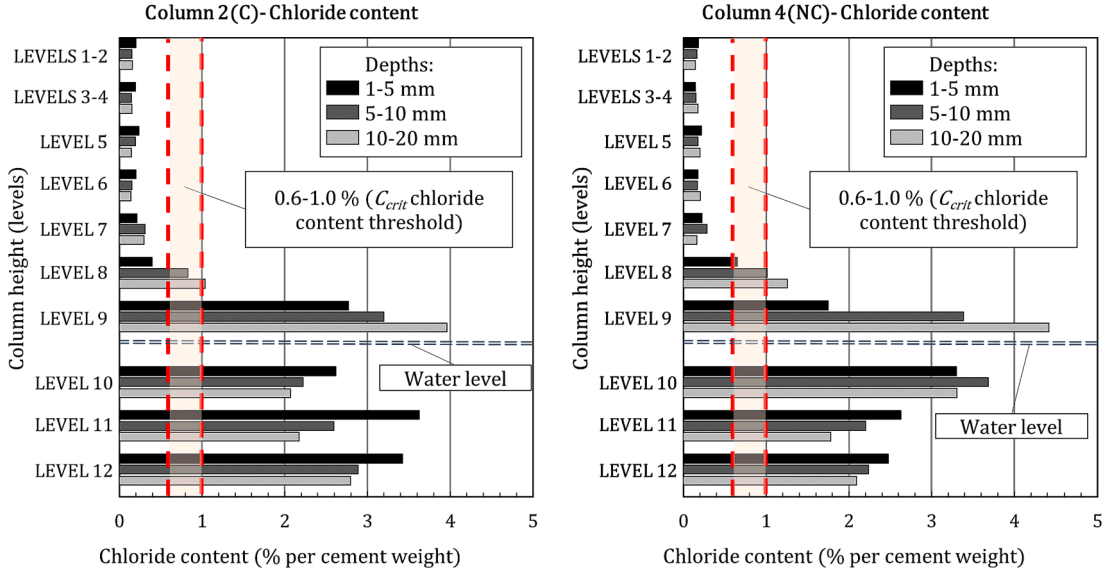

Fig. 12. Chloride concentration profiles at different heights of columns 2 (C-type) and 4 (NC-type).

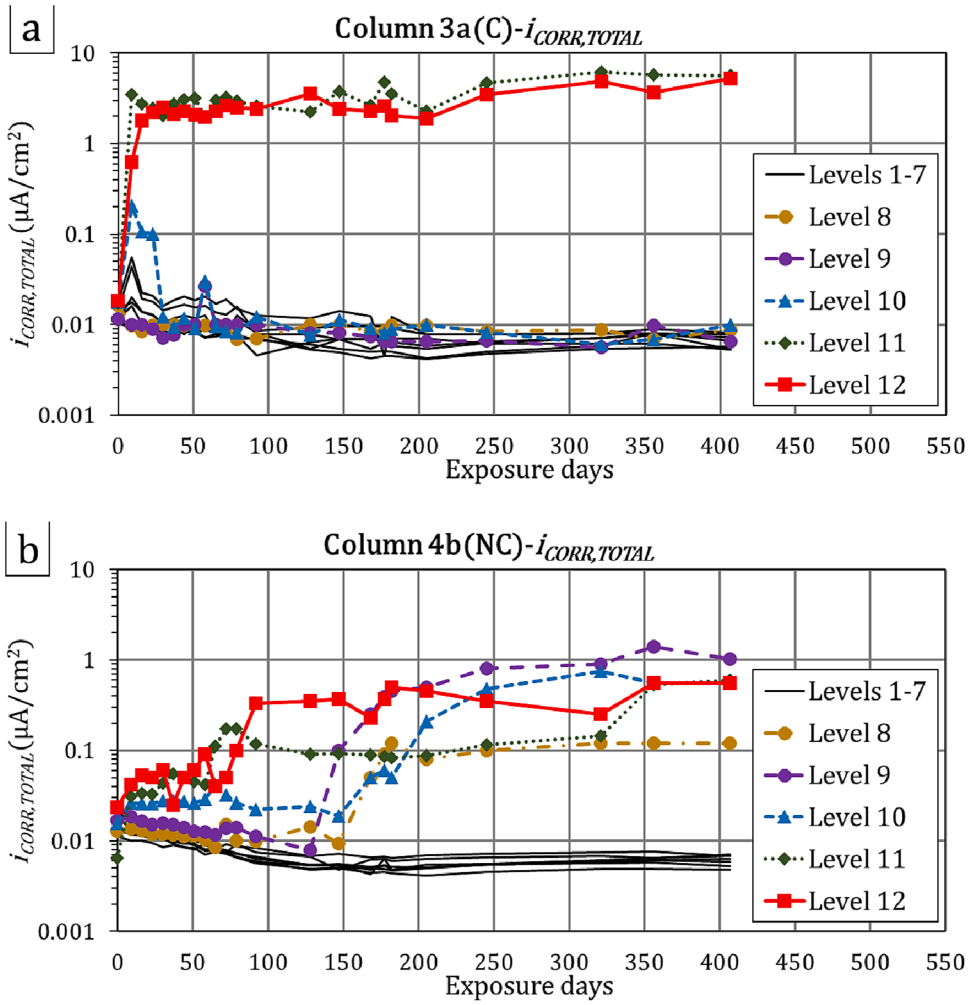

Fig. 13. Corrosion ($i_{CORR,TOTAL}$) evolution in: (a) a column with configuration C (3a) and (b) NC (4b).

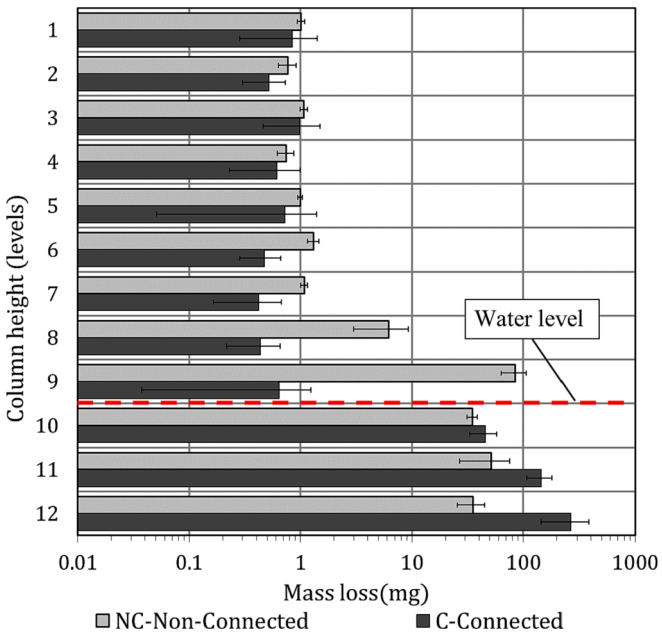

Fig. 14. Mass loss for levels in columns C and NC.

4. In the columns where rebar segments are located at different heights and are not electrically interconnected, maximum corrosion takes place in the aerial zone closest to the water surface. However, in the columns where electrical continuity exists in rebars (where macrocell currents exist), maximum corrosion occurs in immersed zones. This latter case reproduces the real performance of RCS partially immersed in seawater.
5. Macrocell currents lead to electron migration from anodic regions to cathodic ones, which results in chloride ions (negative electrical charge) being drawn by anodic regions (positive electric charge). Consequently, when a macrocell current is present, the chloride diffusion process is also empowered by a migration process, with a 30% higher chloride content around the bars in the anodic regions.

CRediT authorship contribution statement

J.R. Lliso-Ferrando: Conceptualization, Formal analysis, Writing – original draft, Writing – review & editing, Funding acquisition. **J. Soto:** Funding acquisition, Supervision, Writing – review & editing. **I. Gasch:** Formal analysis, Investigation, Writing – review & editing. **M. Valcuende:** Conceptualization, Formal analysis, Funding acquisition, Methodology, Supervision, Writing – review & editing.

Declaration of Competing Interest

The authors declare that they have no known competing financial interests or personal relationships that could have appeared to influence

the work reported in this paper.

Data availability

Data will be made available on request.

Acknowledgements

The authors thank the Spanish Government for Grant PID2020-119744RB-C21 funded by MCIN/AEI/10.13039/501100011033, and the support of the Universitat Politècnica de València. They are also grateful for the predoctoral scholarship granted to Josep Ramon Lliso Ferrando as part of the "Formación de Personal Investigador" programme of the Universitat Politècnica de València (FPI-UPV-2018).

References

[1] B. Touil, F. Ghomari, A. Khelidj, S. Bonnet, O. Amiri, Durability assessment of the oldest concrete structure in the Mediterranean coastline: The Ghazaouet harbour, Mar. Struct. 81 (2022) 103121.
[2] T. Senga Kiesse, S. Bonnet, O. Amiri, A. Ventura, Analysis of corrosion risk due to chloride diffusion for concrete structures in marine environment, Mar. Struct. 73 (2020) 102804.
[3] A.R. Al-Rabiah, Rasheeduzzafar, R. Baggott, Baggott, Durability requirements for reinforced concrete construction in aggressive marine environments, Mar. Struct. 3 (4) (1990) 285–300.
[4] H.P. Chen, Y. Jiang, G. Markou, Structural performance deterioration of corroding reinforced concrete columns in marine environments, Ocean Eng. 262 (2022), 112155, https://doi.org/10.1016/j.oceaneng.2022.112155.
[5] G. Lin, Y. Liu, Z. Xiang, Numerical modeling for predicting service life of reinforced concrete structures exposed to chloride environments, Cem. Concr. Compos. 32 (2010) 571–579, https://doi.org/10.1016/j.cemconcomp.2010.07.012.
[6] A. Zaki, H.K. Chai, D.G. Aggelis, N. Alver, Non-destructive evaluation for corrosion monitoring in concrete: A review and capability of acoustic emission technique, Sensors (Switzerland). 15 (2015) 19069–19101, https://doi.org/10.3390/s150819069.
[7] K. Koulouris, C. Apostolopoulos, Study of the residual bond strength between corroded steel bars and concrete—a comparison with the recommendations of fib model code 2010, Metals (Basel). 11 (5) (2021) 757.
[8] J. Kraľovanec, M. Moravčík, P. Bujňáková, J. Jošt, Indirect determination of residual prestressing force in post-tensioned concrete beam, Materials (Basel). 14 (6) (2021) 1338.
[9] X. Shi, N. Xie, K. Fortune, J. Gong, Durability of steel reinforced concrete in chloride environments: An overview, Constr. Build. Mater. 30 (2012) 125–138, https://doi.org/10.1016/j.conbuildmat.2011.12.038.
[10] D. Qiao, H. Nakamura, Y. Yamamoto, T. Miura, Crack patterns of concrete with a single rebar subjected to non-uniform and localized corrosion, Constr. Build. Mater. 116 (2016) 366–377, https://doi.org/10.1016/j.conbuildmat.2016.04.149.
[11] Y. Liang, L. Wang, Prediction of corrosion-induced cracking of concrete cover: A critical review for thick-walled cylinder models, Ocean Eng. 213 (2020), 107688, https://doi.org/10.1016/j.oceaneng.2020.107688.
[12] H. Zhang, W. Zhang, Z. Yin, Hydrodynamic and dissolved oxygen transport characteristics of an upper and lower water exchange device with regular waves, Ocean Eng. 249 (2022), 110916, https://doi.org/10.1016/j.oceaneng.2022.110916.
[13] A. Costa, J. Appleton, Chloride penetration into concrete in marine environment - Part I: Main parameters affecting chloride penetration, Mater. Struct. Constr. 32 (1999) 252–259, https://doi.org/10.1007/bf02479594.
[14] A. Costa, J. Appleton, Chloride penetration into concrete in marine environment - Part II: Prediction of long term chloride penetration, Mater. Struct. Constr. 32 (1999) 354–359, https://doi.org/10.1007/bf02479594.
[15] L. Zhang, Y.-S. Ji, F. Gao, L. Liu, J. Li, Experimental research and mechanism analysis on chloride ingress at different concrete zone along altitude in marine environment. Part 1. Moisture distribution, Constr. Build. Mater. 180 (2018) 629–642.
[16] M. Shafikhani, S.E. Chidiac, Quantification of concrete chloride diffusion coefficient – A critical review, Cem. Concr. Compos. 99 (2019) 225–250, https://doi.org/10.1016/j.cemconcomp.2019.03.011.
[17] A.V. Saetta, R.V. Scotta, R.V. Vitaliani, Analysis of Chloride Diffusion into Partially Saturated Concrete, Mater. J. 90 (1993) 441–451.
[18] A.A. Sagüés, M.A. Pech-Canul, A.K.M. Shahid Al-Mansur, Corrosion macrocell behavior of reinforcing steel in partially submerged concrete columns, Corros. Sci. 45 (2003) 7–32, https://doi.org/10.1016/S0010-938X(02)00087-2.
[19] Z. Yu, Y. Chen, P. Liu, W. Wang, Accelerated simulation of chloride ingress into concrete under drying-wetting alternation condition chloride environment, Constr. Build. Mater. 93 (2015) 205–213, https://doi.org/10.1016/j.conbuildmat.2015.05.090.
[20] C. Lu, Y. Gao, Z. Cui, R. Liu, Experimental Analysis of Chloride Penetration into Concrete Subjected to Drying-Wetting Cycles, J. Mater. Civ. Eng. 27 (2015) 1–10, https://doi.org/10.1061/(asce)mt.1943-5533.0001304.
[21] A. Aguilar, A.A. Sagues, R.G. Powers, Corrosion measurements of reinforcing steel in partially submerged concrete slabs, ASTM Spec. Tech. Publ. (1990) 66–85, https://doi.org/10.1520/stp25016s.
[22] M. Khanzadeh Moradllo, S. Sadati, M. Shekarchi, Quantifying maximum phenomenon in chloride ion profiles and its influence on service-life prediction of concrete structures exposed to seawater tidal zone – A field oriented study, Constr. Build. Mater. 180 (2018) 109–116, https://doi.org/10.1016/j.conbuildmat.2018.05.284.
[23] H. Chang, S. Mu, D. Xie, P. Wang, Influence of pore structure and moisture distribution on chloride "maximum phenomenon" in surface layer of specimens exposed to cyclic drying-wetting condition, Constr. Build. Mater. 131 (2017) 16–30, https://doi.org/10.1016/j.conbuildmat.2016.11.071.
[24] H. Chang, Z. Zhang, Z. Ma, Y. Ji, X. Huang, Permeation Characteristics and Surface Accumulation of Chloride in Different Zones of Concrete along Altitude in Marine Environments, Crystals. 11 (2021). https://doi.org/https://doi.org/10.3390/cryst11070722.
[25] P. Liu, Z. Yu, Z. Lu, Y. Chen, X. Liu, Predictive convection zone depth of chloride in concrete under chloride environment, Cem. Concr. Compos. 72 (2016) 257–267, https://doi.org/10.1016/j.cemconcomp.2016.06.011.
[26] K. Li, J. Zeng, L. Tang, H. Erndahl, P. Castro, B. Mette, R. Geiker, M. Thostrup, P. Zhang, S. Surana, R. Maddalena, J. Wang, B.F. Martirena-herna, C.A. Ve, G. Geng, K. Kovler, S. Wang, F. Martirena-hernandez, Long-term field exposure of structural concretes in marine environment : state-of-the-art review by RILEM TC, 2 (2022). https://doi.org/10.1617/s11527-022-02027-2.
[27] L. Bertolini, B. Elsener, P. Pedeferri, E. Redaelli, R.B. Polder, Corrosion of Stell in Concrete: Prevention, Diagnosis and Repair, Wiley-VCH, Weinheim, Germany, 2013.
[28] A. Brenna, F. Bolzoni, S. Beretta, M. Ormellese, Long-term chloride-induced corrosion monitoring of reinforced concrete coated with commercial polymer-modified mortar and polymeric coatings, Constr. Build. Mater. 48 (2013) 734–744, https://doi.org/10.1016/j.conbuildmat.2013.07.099.
[29] J. Williamson, O.B. Isgor, The effect of simulated concrete pore solution composition and chlorides on the electronic properties of passive films on carbon steel rebar, Corros. Sci. 106 (2016) 82–95, https://doi.org/10.1016/j.corsci.2016.01.027.
[30] A. Poursaee, Temperature dependence of the formation of the passivation layer on carbon steel in high alkaline environment of concrete pore solution, Electrochem. Commun. 73 (2016) 24–28, https://doi.org/10.1016/j.elecom.2016.10.003.
[31] A. Poursaee, Corrosion of steel in concrete structures, in: Corrosion of Steel in Concrete Structures, Elsevier, 2016, pp. 19–33.
[32] P. Ghods, O.B. Isgor, G. McRae, T. Miller, The effect of concrete pore solution composition on the quality of passive oxide films on black steel reinforcement, Cem. Concr. Compos. 31 (2009) 2–11, https://doi.org/10.1016/j.cemconcomp.2008.10.003.
[33] M. Pourbaix, Atlas of chemical and electrochemical equilibria in aqueous solutions, National Association of Corrosion Engineers, Houston, Texas, USA (1974), https://doi.org/10.4028/www.scientific.net/msf.251-254.143.
[34] U. Angst, B. Elsener, C.K. Larsen, Ø. Vennesland, Critical chloride content in reinforced concrete - A review, Cem. Concr. Res. 39 (2009) 1122–1138, https://doi.org/10.1016/j.cemconres.2009.08.006.
[35] W. Li, L. Guo, Peridynamic investigation of chloride diffusion in concrete under typical environmental factors, Ocean Eng. 239 (2021), 109770, https://doi.org/10.1016/j.oceaneng.2021.109770.
[36] C. Andrade, I.R. Maribona, S. Feliu, J.A. González, S. Feliu, The effect of macrocells between active and passive areas of steel reinforcements, Corros. Sci. 33 (2) (1992) 237–249.
[37] J.R. Lliso-Ferrando, I. Gasch, A. Martínez-Ibernón, M. Valcuende, Effect of macrocell currents on rebar corrosion in reinforced concrete structures exposed to a marine environment, Ocean Eng. 257 (2022) 111680.
[38] C. Andrade, P. Garcés, I. Martínez, Galvanic currents and corrosion rates of reinforcements measured in cells simulating different pitting areas caused by chloride attack in sodium hydroxide, Corros. Sci. 50 (2008) 2959–2964, https://doi.org/10.1016/j.corsci.2008.07.013.
[39] B. Elsener, Macrocell corrosion of steel in concrete - Implications for corrosion monitoring, Cem. Concr. Compos. 24 (2002) 65–72, https://doi.org/10.1016/S0958-9465(01)00027-0.
[40] L. Chen, R.K.L. Su, Corrosion rate measurement by using polarization resistance method for microcell and macrocell corrosion: Theoretical analysis and experimental work with simulated concrete pore solution, Constr. Build. Mater. 267 (2021), 121003, https://doi.org/10.1016/j.conbuildmat.2020.121003.
[41] S. Qian, J. Zhang, D. Qu, Theoretical and experimental study of microcell and macrocell corrosion in patch repairs of concrete structures, Cem. Concr. Compos. 28 (2006) 685–695, https://doi.org/10.1016/j.cemconcomp.2006.05.010.
[42] J.R. Lliso-Ferrando, I. Gasch, A. Martínez-Ibernón, M. Valcuende, Macrocell Corrosion Currents in Simulated Concrete Pore Solution and Reinforced Concrete, Int. J. Concr. Struct. Mater. 17 (2023), https://doi.org/10.1186/s40069-022-00576-y.
[43] G.S. Duffó, S.B. Farina, Electrochemical behaviour of steel in mortar and in simulated pore solutions: Analogies and differences, Cem. Concr. Res. 88 (2016) 211–216, https://doi.org/10.1016/j.cemconres.2016.07.007.
[44] A.B. Revert, K. Hornbostel, K. De Weerdt, M.R. Geiker, Macrocell corrosion in carbonated Portland and Portland-fly ash concrete - Contribution and mechanism, Cem. Concr. Res. 116 (2019) 273–283, https://doi.org/10.1016/j.cemconres.2018.12.005.
[45] C.M. Hansson, A. Poursaee, A. Laurent, Macrocell and microcell corrosion of steel in ordinary Portland cement and high performance concretes, Cem. Concr.

Compos. 36 (2006) 2098–2102, https://doi.org/10.1016/j.cemconres.2006.07.005.
[46] K.V. Subramaniam, M. Bi, Investigation of steel corrosion in cracked concrete : Evaluation of macrocell and microcell rates using Tafel polarization response, Corros. Sci. 52 (2010) 2725–2735, https://doi.org/10.1016/j.corsci.2010.04.030.
[47] P. Rodríguez, E. Ramirez, S. Feliu, J.A. Gonzalez, W. López, Significance of coplanar macrocells to corrosion in concrete-embedded steel, Corrosion. 55 (1999) 319–325, https://doi.org/10.5006/1.3283994.
[48] M. Valipour, M. Shekarchi, P. Ghods, Comparative studies of experimental and numerical techniques in measurement of corrosion rate and time-to-corrosion-initiation of rebar in concrete in marine environments, Cem. Concr. Compos. 48 (2014) 98–107, https://doi.org/10.1016/j.cemconcomp.2013.11.001.
[49] F. Micelli, L. Candido, E. Vasanelli, M.A. Aiello, G. Plizzari, Effects of short fibers on the long-term behavior of RC/FRC beams aged under service loading, Appl. Sci. 9 (12) (2019) 2540.
[50] E. Chen, C.G. Berrocal, I. Löfgren, K. Lundgren, Correlation between concrete cracks and corrosion characteristics of steel reinforcement in pre-cracked plain and fibre-reinforced concrete beams, Mater. Struct. Constr. 53 (2020), https://doi.org/10.1617/s11527-020-01466-z.
[51] J. Shen, X. Gao, B. Li, K. Du, R. Jin, W. Chen, Y. Xu, Damage evolution of RC beams under simultaneous reinforcement corrosion and sustained load, Materials (Basel). 12 (2019) 1–16, https://doi.org/10.3390/ma12040627.
[52] G. Triantafyllou, T. Rousakis, A. Karabinis, Corroded RC beams at service load before and after patch repair and strengthening with NSM CFRP strips, Buildings. 9 (3) (2019) 67.
[53] M.T. Walsh, A.A. Sagüés, Steel corrosion in submerged concrete structures-Part 1: Field Observations and Corrosion Distribution Modeling, Corrosion. 72 (2016) 518–533, https://doi.org/10.5006/1945.
[54] M.T. Walsh, A.A. Sagüés, Steel corrosion in submerged concrete structures-Part 2: Modeling of corrosion evolution and control, Corrosion. 72 (2016) 665–678, https://doi.org/10.5006/1944.
[55] ASTM International, D1141-98 (2021) Standard Practice for the Preparation of Substitute Ocean Water. 2021.
[56] AENOR, UNE-EN 12390-3:2009. Ensayos de hormigón endurecido. Parte 3: Determianción de la resistencia a compresión de probetas, UNE-EN (2009).
[57] AENOR, UNE-EN 83980:2014. Determinación de la absorción de agua, la densidad y la porosidad accesible al agua del hormigón. (2014).
[58] AENOR, UNE-EN 83982. Determinación de la absorción de agua por capilaridad del hormigón endurecido. Método Fagerlund, (2008).
[59] AENOR, UNE-EN 83981:2008. Determinación de la permeabilidad al oxígeno del hormigón endurecido. (2008).
[60] Nordtest, NT Build 492. Rapid Chloride Migration Test (RCMT), Nord. Method. Nord. Coop. (1999) 1–8.
[61] A.E. de N. y C. AENOR, UNE-EN 12390-11:2019. Ensayos en Hormigón Endurecido. Parte 11 : Determinación de la resistencia a los cloruros del hormigón , difusión unidireccional. (2019).
[62] AENOR, UNE 112072:2011. Determinación de la velocidad de corrosión de armaduras en laboratorio mediante medida de la resistencia a la polarización. (2011).
[63] American Society of Testing Materials (ASTM), ASTM G1-03Standard Practice for Preparing, Cleaning, and Evaluating Corrosion Test Specimens., Est Conshohocken. 1999.
[64] A.A. Almusallam, A.S. Al-Gahtani, A.R. Aziz, F.H. Dakhil, Rasheeduzzafar, Effect of reinforcement corrosion on flexural behaviour of concrete slabs, J. Mater. Civ. Eng. 8 (1996) 123–127.
[65] C.E.T. Balestra, A.Y. Nakano, G. Savaris, R.A. Medeiros-Junior, Reinforcement corrosion risk of marine concrete structures evaluated through electrical resistivity: Proposal of parameters based on field structures, Ocean Eng. 187 (2019), 106167, https://doi.org/10.1016/j.oceaneng.2019.106167.
[66] N.R. Buenfeld, C.L. Newman, C.L. Page, The resistivity of mortars immersed in seawater, Cem. Concr. Res. 16 (1986) 511–524, https://doi.org/10.1016/0008-8846(86)90089-X.
[67] N. Gartner, T. Kosec, A. Legat, Monitoring the corrosion of steel in concrete exposed to a marine environment, Materials (Basel). 13 (2) (2020) 407.
[68] C. Andrade, C. Alonso, J. Gulikers, R. Polder, R. Cigna, M. Vennesland, A. Salta, B. E. Raharinaivo, RILEM TC-154-EMC: Electrochemical Techniques for Measuring Metallic Corrosion. Test methods for on-site corrosion rate measurement of steel reinforcement in concrete by means of the polarization resistance method, Mater. Struct. Constr. 37 (2004) 623–643, https://doi.org/10.1617/13952.
[69] C. Andrade, M.C. Alonso, J.A. González, An initial effort to use the corrosion rate measurements for estimating rebar durability, in: N.S. Berke, V. Chaker, D. Whiting (Eds.), Corros. Rates Steel Concr. ASTM STP 1065, American Society of Testing and Materials, Philadelphia, USA. 1990.
[70] G. Quincot, M. Azenha, J. Barros, R. Faria, State of the Art – Methods to Measure Moisture in Concrete, Proj. Investig. …. (2011) 40. http://paginas.fe.up.pt/~selco/wp-content/uploads/2014/02/Relatorio_1.pdf.
[71] J. Hundt, J. Buschmann, Moisture measurement in concrete, Matériaux Constr. 4 (1971) 253–256, https://doi.org/10.1007/bf02478952.
[72] NORDTEST; Nordic Cooperation, NT Build 208. Chloride content by Volhard titration. Nord. Method. 3 (1996). 1–4.
[73] R.B. Polder, Critical chloride content for reinforced concrete and its relationship to concrete resistivity, Mater. Corros. 60 (2009) 623–630, https://doi.org/10.1002/maco.200905302.
[74] W. Chalee, C. Jaturapitakkul, P. Chindaprasirt, Predicting the chloride penetration of fly ash concrete in seawater, Mar. Struct. 22 (2009) 341–353, https://doi.org/10.1016/j.marstruc.2008.12.001.
[75] Y. Gao, Y. Zheng, J. Zhang, J. Wang, X. Zhou, Y. Zhang, Randomness of critical chloride concentration of reinforcement corrosion in reinforced concrete flexural members in a tidal environment, Ocean Eng. 172 (2019) 330–341, https://doi.org/10.1016/j.oceaneng.2018.11.038.
[76] D. Li, L.-Y. Li, X. Wang, Chloride diffusion model for concrete in marine environment with considering binding effect, Mar. Struct. 66 (2019) 44–51.
[77] Q. Liu, L. Sun, X. Zhu, L. Xu, G. Zhao, Chloride transport in the reinforced concrete column under the marine environment: Distinguish the atmospheric, tidal-splash and submerged zones, Structures. 39 (2022) 365–377, https://doi.org/10.1016/j.istruc.2022.03.041.